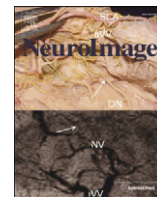




Contents lists available at ScienceDirect

NeuroImage

journal homepage: www.elsevier.com/locate/ynimg

BOLD responses to different temporal frequency stimuli in the lateral geniculate nucleus and visual cortex: Insights into the neural basis of fMRI

Cecil Chern-Chyi Yen^{a,b}, Mitsuhiro Fukuda^a, Seong-Gi Kim^{a,b,c,*}

^a Neuroimaging Laboratory, Department of Radiology, University of Pittsburgh, Pittsburgh, PA 15203, USA

^b Department of Bioengineering, University of Pittsburgh, Pittsburgh, PA 15203, USA

^c Department of Neurobiology, University of Pittsburgh, Pittsburgh, PA 15203, USA

ARTICLE INFO

Article history:

Received 18 December 2010

Revised 8 June 2011

Accepted 9 June 2011

Available online 17 June 2011

Keywords:

BOLD

fMRI

Temporal frequency

LGN

Visual cortex

Neural basis

Neural activity

ABSTRACT

The neural basis of the blood oxygenation level dependent (BOLD) functional magnetic resonance imaging (fMRI) remains largely unknown after decades of research. To investigate this issue, the unique property of the temporal frequency tuning that could separate neural input and output in the primary visual cortex was used as a model. During moving grating stimuli of 1, 2, 10 and 20 Hz temporal frequencies, we measured 9.4-T BOLD fMRI responses simultaneously in the primary visual cortex of area 17 (A17) and area 18 (A18), and the lateral geniculate nucleus (LGN) of isoflurane-anesthetized cat. Our results showed that preferred temporal frequencies of the BOLD responses for A17, A18 and LGN were 3.1 Hz, 4.5 Hz and 6.0 Hz, respectively, which were comparable to the previously reported electrophysiological data. Additionally, the difference of BOLD response onset time between LGN and A17 was 0.5 s, which is 18 times larger than the difference of neural activity onset time between these areas. We then compared the frequency-dependent BOLD fMRI response of A17 with tissue partial pressure of oxygen (pO_2) and electrophysiological data of the same animal model reported by Viswanathan and Freeman (Nature Neuroscience, 2007). The BOLD tuning curve resembled the low frequency band (<12 Hz) of local field potential (LFP) tuning curve rather than spiking activity, gamma band (25–90 Hz) of LFP, and tissue pO_2 tuning curves, suggesting that the BOLD fMRI signal relates closer to low frequency LFP.

© 2011 Elsevier Inc. All rights reserved.

Introduction

Functional magnetic resonance imaging (fMRI) with blood oxygenation level dependent (BOLD) contrast is one of the most important noninvasive modalities to study the function of the human brain (Bandettini et al., 1992; Kwong et al., 1992; Ogawa et al., 1992). Many neuroscientists and psychologists rely on BOLD fMRI to decode sophisticated neural processes in different brain areas. Nevertheless, the connection between the BOLD signal and the underlying neural activity is still under debate, even after decades of research (Ekstrom, 2010). Without a comprehensive understanding of how the BOLD signal relates to different aspects of neural activities, BOLD fMRI cannot be correctly interpreted.

Neural activity can be broadly classified into local field potentials (LFP) and spiking activity; LFP is generally believed to represent synaptic activity including neural input (Khawaja et al., 2009; Mitzdorf, 1985), while spiking activity represents supra-threshold neural output. It has been reported that the BOLD fMRI response is

correlated with i) underlying LFP rather than spiking activity (Logothetis et al., 2001), ii) mostly spiking activity (Heeger and Ress, 2002; Rees et al., 2000), or iii) both LFP and spiking activity (Mukamel et al., 2005). Because spiking activity always occurs together with LFP, it is difficult to separate their contributions to the BOLD response in most circumstances. Decoupling between LFP and spiking activity, however, can be achieved by using different temporal frequency properties between thalamocortical input and cortical output (Viswanathan and Freeman, 2007). The thalamocortical input driven by lateral geniculate nucleus (LGN), the main visual relay nucleus located in the thalamus, has a higher temporal frequency preference (Derrington and Fuchs, 1979) than spiking activity in feline cortical area 17 (A17) and area 18 (A18) (Bisti et al., 1985). Note that although feline A18 shares many similarities in neuronal and vascular properties as A17, the temporal frequency preference (tuning) of A18 is slightly higher than A17 (Bisti et al., 1985). Thus, cortical input and output in primary visual cortex dissociate at high temporal frequency stimulation. Using this property, Viswanathan and Freeman (2007) measured both neural activity and tissue partial pressure of oxygen (pO_2) with a polarographic oxygen sensor in feline A17, and found a change in pO_2 even in the absence of spiking activity during high temporal frequency stimulation. Assuming that the BOLD fMRI signal is analogous to pO_2 change, Viswanathan and Freeman

* Corresponding author at: Neuroimaging Lab, Department of Radiology, 3025 East Carson Street, University of Pittsburgh, Pittsburgh, PA 15203, USA. Fax: +1 412 383 6799.

E-mail address: kimsg@pitt.edu (S.-G. Kim).

(2007) suggested that the BOLD fMRI reflects LFP. However, this inference may not be valid due to the non-linear relationship between tissue pO_2 and BOLD signal (Vazquez et al., 2010), and contributions of cerebral blood volume (CBV) to the BOLD signal (Ogawa et al., 1998). Therefore, it is important to perform BOLD fMRI during different temporal frequency stimuli for addressing neural sources of the BOLD signal.

In the present study, we obtained BOLD fMRI in feline early visual system (LGN, A17 and A18) at 9.4 T during four different temporal frequency stimulations of 1, 2, 10 and 20 Hz. The BOLD response versus temporal frequency (i.e., temporal frequency tuning curve) was determined. Then, frequency tuning curves and dynamics of BOLD fMRI in A17, A18 and LGN were compared with corresponding spiking activity data reported in the literature (Allison et al., 2001; Baker and Issa, 2005; Bisti et al., 1985; DeAngelis et al., 1993; Derrington and Fuchs, 1979) in order to determine the consistency between fMRI and neural activity. Finally, the BOLD tuning curve of A17 was compared to neural and pO_2 tuning curves in the same animal model reported by Viswanathan and Freeman (2007) for examining the neural source of BOLD fMRI. Part of the work was presented in abstract forms (Yen et al., 2009, 2010).

Materials and methods

Procedures of animal preparation

Eight adolescent cats, weighted between 1.14 and 1.68 kg, were used under an animal protocol approved by the Institutional Animal Care and Use committee at the University of Pittsburgh. Atropine sulfate (0.05 mg/kg, IM) was injected to suppress mucus secretion. The cat was then anesthetized with an intramuscular injection of a ketamine (10–20 mg/kg)/xylazine (0.2 mg/kg) cocktail and intubated for mechanical ventilation with a pressure-driven ventilator (24–28 stroke/min). Isoflurane gaseous anesthesia was maintained at 1.5% in a mixture of $N_2/O_2 = 0.7/0.3$ during surgical preparation. A cephalic intravenous catheter was placed for infusion of supplemental fluids (5% dextrose) with pancuronium bromide (0.15–0.2 mg/kg/h). The pupils were dilated by 1% tropicamide ophthalmic solution and nictitating membranes were retracted by 2.5% phenylephrine hydrochloride. Contact lenses were then fitted to both eyes. The cat was placed in a custom-built cradle and restrained in normal postural position with ear and a bite bars. Rectal temperature was maintained between 37.7 and 38.3 °C by a feedback-controlled water circulator. End-tidal CO_2 was monitored by a capnometer and maintained in the range of 3.4–3.8% by adjusting the volume and/or rate of the ventilator. Vital signs were displayed and recorded using a polygraph system (BIOPAC, Goleta, CA, USA). During functional studies, the isoflurane level was maintained at 0.9–1.1%. In addition to isoflurane, functional sessions were also performed under mixture of pentobarbital (1.5 mg/kg/h) and fentanyl (10 μ g/kg/h) in two cats to examine the influence of anesthesia on temporal frequency-dependent fMRI responses.

Paradigm of visual stimulation

Four temporal frequencies including 1, 2, 10 and 20 Hz of vertical sinusoid-gratings were projected on a frosted glass screen positioned 9 to 11 cm away from the cat eyes. Thus, the stimulation spanned approximately 54°–67° in the visual field of view (θ in Fig. 1A) for the cat. Visual stimuli were generated by a personal computer using custom Matlab script (MathWorks, Natick, MA, USA) with Psychophysics Toolbox extensions (Brainard, 1997). The frame-dropping rate for our stimuli, reported by Psychophysics Toolbox, was less than 0.1% for all experiments. Due to the electronic property of our LCD projector (NEC Display Solutions, Itasca, IL, USA; model: MT-1055; resolution 1024 \times 768 pixels and 60 Hz refresh rate), the peak-to-peak

intensity had to be reduced to 60% of the maximum intensity such that a proper sinusoid pattern was generated for all temporal frequencies. The accuracy of the generated sinusoid pattern was examined by a fast charge-coupled device (>100 frame/s). The luminance for the crest and the trough of the sinusoid pattern was ~ 25 cd/m² and ~ 4 cd/m² as determined by a chroma meter. Each epoch of the stimulation paradigm consisted of 4-s unidirectional moving sinusoidal gratings and 20-s stationary gratings (see Fig. 1A). The spatial frequency, defined as number of cycles of a sinusoidal grating that spans 1° of the visual angle, was fixed to 0.15 cycle/degree for all temporal frequency stimuli. A total of 32 epochs with four temporal frequencies were pseudo-randomized within each fMRI run, and ≥ 15 runs were performed.

Protocol of MRI acquisition

The cat was placed inside a 9.4-T/31-cm horizontal bore magnet interfaced to a Unity INOVA console (Varian, Palo Alto, CA, USA). The actively shielded 12-cm diameter gradient insert reached its maximum gradient strength of 40 Gauss/cm within 120 μ s. A custom-built butterfly-shaped surface coil with length \times width \times depth = 5 \times 3 \times 1.5 cm³ was used. This coil was etched on a flexible Teflon-printed circuit board (Rogers Corporation, Rogers, CT, USA) mounted on a half cylinder acryl plate. Three-plane scout images were acquired for the initial positioning of the imaging slices. An automatic three-dimensional (3-D) gradient shimming routine was used to minimize the magnetic field inhomogeneity over the imaging slices, yielding a water spectral linewidth of <25 Hz. To precisely prescribe the slice position of fMRI studies, a 3-D venographic image with isotropic resolution of 78 μ m³, which delineated veins and gray matter, was obtained using a 3-D gradient-recalled echo imaging technique with flow compensation (Park et al., 2008). To acquire anatomical reference for fMRI, myelin-enhanced T_1 -weighted images were obtained using a multiple-segment inversion-recovery turbo fast low angle shot (IR-TurboFLASH) sequence with in-plane resolution of 156 μ m² (Kim and Kim, 2011) in the same imaging slices as fMRI. Inversion time was set to the nulling point of the gray matter at 9.4 T.

For fMRI studies, two or four adjacent coronal 2-mm-thick images covering both the primary visual cortex and LGN were acquired using a partial-Fourier gradient-recalled echo-planar imaging (GR-EPI) sequence (Jesmanowicz et al., 1998) with a 4.096-ms apodized sinc RF excitation pulse. The RF power was determined as the average of the optimal RF power at the visual cortex and LGN. The imaging parameters were: field of view = 40 \times 30 mm², matrix size = 128 \times 60 (with phase-encoding overscan lines of 12) reconstructed to 128 \times 96, in-plane resolution = 313 \times 313 μ m², readout echo spacing = 0.4998 ms, TE = 20 ms, and TR = 1 s. To minimize Gibbs ringing artifacts, the missing 36 k-space lines were synthesized by the projection onto convex set theory (Haacke et al., 1991). A data collection order of imaging slices was reversed for every other run to cancel out the timing error between slices after averaging.

Generation of fMRI maps

Before doing any statistical tests, a linear detrend and a Fermi high-pass temporal filter with a radius of 0.021 Hz and a width of 0.001 Hz were applied to minimize signal fluctuations induced by low frequency signal drifting (<0.021 Hz). Additionally, a Gaussian notch temporal filter with a center frequency of 0.429 ± 0.019 Hz (mean \pm SD; depending on the respiration rate of each run) and a bandwidth of 0.009 Hz was applied to reduce the breathing-related fluctuation. The frequency of the stimuli was 0.042 Hz, which was not affected by the notch filter or the Fermi high-pass filter. The first few epochs of each run were discarded because of the progression reaching a steady state condition and the potential influence of acoustic noise on the visual system via indirect projection from the auditory system (Moelker and

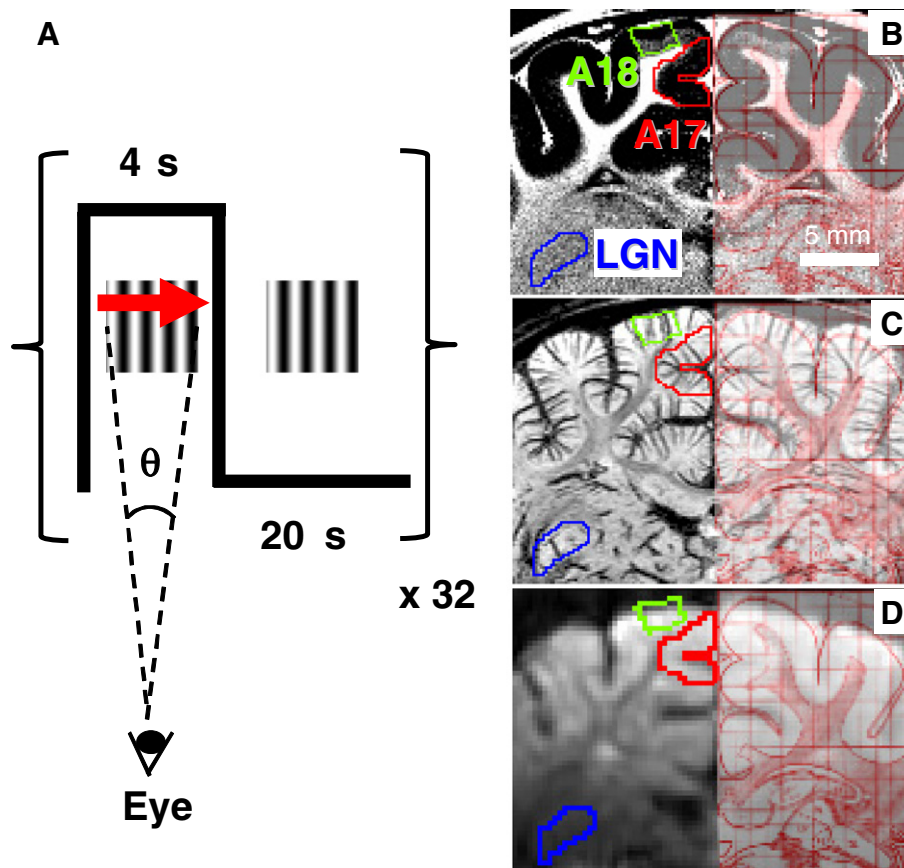


Fig. 1. Stimulus paradigm and regions of the early visual areas. (A) Each stimulus epoch consisted of 4-s moving sinusoidal gratings and 20-s stationary gratings. The temporal frequency of moving sinusoidal gratings (unit: cycles/sec) is defined as number of cycles of a grating passing at one visual point per 1 s, and spatial frequency (unit: cycles/deg) is defined as number of cycles of a sinusoidal grating that span 1° of the visual angle, θ . Since the velocity of the moving sinusoidal grating is linearly proportional to the temporal frequency when the spatial frequency is fixed, higher temporal frequency corresponds to faster movement of the sinusoidal grating. (B–D) Regions of interest (ROI) of A17 (red), A18 (green) and LGN (blue) were obtained in both hemispheres, but overlaid on T_1 -weighted (B), T_2^* -weighted (C), and baseline EPI images (D) only on the left hemisphere for display. The same ROIs were used for further data analyses, and shown in subsequent figures. The cat brain atlas (Reinoso-Suárez, 1961) of a corresponding slice was overlaid on the right hemisphere of the three images (B–D). In the T_1 -weighted image (B), in which gray matter signal is almost nulled, white matter and cerebrospinal fluid (CSF) appear white. In the T_2^* weighted image (C), vein, gray matter, and white matter appear dark, white, and gray, respectively. LGN was identified in the lower lateral sub-cortex of the image surrounded by grayish optical radiation, optic nerve and dark veins in the T_2^* weighted image, and appears a little darker than the surrounding region in the T_1 -weighted image. Note that the lateral boundaries of A17 and A18 ROIs were chosen to be parallel to the penetrating veins in T_2^* weighted image. The baseline EPI image (D) shows no distortion and matches well with the atlas and conventional anatomic images.

Pattynama, 2003). To determine the proper hemodynamic response function (HRF), an independent component analysis was carried out using MELODIC in FSL (FMRIB's Software Library) (Beckmann and Smith, 2004) and a single gamma HRF was determined from the time course of the first independent component. All fMRI activation maps were calculated using FEAT in FSL with cluster significance threshold of $p = 0.05$ (Smith et al., 2004). No additional spatial or temporal filtering was applied. Activation maps generated by FSL were overlaid on the baseline EPI images of each animal using MRIcron (Rorden et al., 2007).

Quantitative region of interest analysis

Time course analysis

As shown in Figs. 1B–D, regions of interest (ROI) of A17 (red) and A18 (green) were defined on IR TurboFLASH image (Fig. 1B), while the ROI of LGN (blue) was defined on venographic image (Fig. 1C), but avoiding large veins, according to the cat brain atlas (Reinoso-Suárez, 1961) using STIMULATE (Strupp, 1996) and ImageJ (Abramoff et al., 2004) programs. For better visualization, a high-pass Gaussian spatial filter was applied to anatomical images to reduce the signal variation induced by B_1 inhomogeneity. The functional image acquired by the partial-Fourier GR-EPI sequence (Fig. 1D) showed minimal geometric distortion near the ROIs comparing to the anatomical images using

the same overlay of the cat brain atlas (Reinoso-Suárez, 1961) on the right hemisphere as a visual guide. Furthermore, functional image showed good contrast and no partial Fourier acquisition induced Gibbs ringing artifact (Fig. 1D). BOLD time courses of the three aforementioned ROIs were extracted from the raw data in each cat and then averaged across all isoflurane-anesthetized cats.

To analyze the dynamic property of fMRI responses in three visual areas, time courses were first linearly interpolated to 0.2 s temporal resolution, then the onset and peak times were determined as the point at which 10% and 90% of the maximum response was attained for each isoflurane-anesthetized cat (Jin and Kim, 2008). The interval of the interpolation was determined empirically. A two-tailed paired t-test was used to determine timing differences between areas.

Frequency tuning curve

Temporal frequency tuning curves were generated for each ROI. The BOLD fMRI responses were averaged from 5 to 8 s after stimulation onset for each temporal frequency, and then normalized by the maximum fMRI response of each ROI in order to minimize inter-animal variations. Then, the temporal frequency tuning curve was obtained by plotting the normalized response vs. the temporal frequency for each cat, and averaged across all isoflurane-anesthetized cats. The preferred frequency, i.e. the temporal frequency of the maximum response, was

obtained by fitting normalized BOLD responses of all eight cats vs. the logarithm of four temporal frequencies with a Gaussian distribution (Allison et al., 2001) using Ezyfit toolbox in Matlab (Moisy, 2011). The map of preferred frequency was generated by finding the preferred frequency of each pixel. Pixels were excluded from fitting if no significant activation was found in all four temporal frequencies and were removed from display if the correlation coefficient of the fitting was lower than 0.3.

Results

Spatiotemporal characteristics of BOLD responses for various temporal frequency stimuli

To compare spatial patterns of BOLD responses to four temporal frequency stimuli, BOLD fMRI activation maps were overlaid on the averaged baseline GR-EPI image in one isoflurane-anesthetized cat (Figs. 2A–D). ROIs of A17 (black), A18 (green) and LGN (blue) were defined as described in the Materials and methods section (see Figs. 1B–D). Positive BOLD responses to 1 Hz (Fig. 2A), 2 Hz (Fig. 2B) and 10 Hz (Fig. 2C) stimulation were mainly found in the LGN, A17 and A18 and had similar patterns with slight variations. For 20 Hz stimulation (Fig. 2D), activation areas of A17 and A18 were smaller compared to that of lower frequencies, while the activation area of LGN was maintained for all frequencies. It should be noted that activation in the superior colliculus (white arrowhead) or pulvinar (yellow arrowhead) were not observed in all cats, thus, they were not included for further analyses.

The distinct BOLD response to various temporal frequency stimuli can be further illustrated by comparing averaged areal time courses for eight isoflurane-anesthetized cats as shown in Figs. 2E–G. In A17 (Fig. 2E), the BOLD fMRI response to 20 Hz stimulation is the lowest (black), while the three other temporal frequencies exhibit similar

amplitudes. In A18 (Fig. 2F), responses to 2 Hz (green) and 10 Hz (blue) have higher amplitudes than 1 Hz (red) and 20 Hz (black). In LGN (Fig. 2G), the response to 10 Hz stimulation has the highest, while 1 Hz stimulation induces the lowest amplitude; time courses with 2 Hz and 20 Hz stimulation are almost identical. Comparing these three areas, LGN always has the highest BOLD response for all temporal frequency stimuli.

To examine the dynamic response of the BOLD signal in the early visual system, normalized BOLD time courses of A17, A18 and LGN were obtained for 2 Hz stimulation (Fig. 3). The dynamic property of the BOLD response induced by 2 Hz was similar to that of 1 and 10 Hz, while the 20 Hz time course was not analyzed for temporal characteristics due to its small amplitude in A17 and A18. The BOLD response of LGN increased earlier and reached the peak earlier than A17 and A18. The onset time of A17, A18 and LGN (horizontal line at $y = 0.1$ in Fig. 3) was 2.3 ± 0.4 , 2.3 ± 0.7 and 1.8 ± 0.6 s (mean \pm SD, $n = 8$ isoflurane-anesthetized cats), respectively. The onset time of LGN was significantly earlier than both A17 ($p = 0.022$, same or earlier in 8 out of 8 cats) and A18 ($p = 0.034$, same or earlier in 7 out of 8 cats); the onset time of A17 and A18 was not significantly different ($p = 0.84$). The peak time of A17, A18 and LGN (horizontal line at $y = 0.9$ in Fig. 3) was 5.4 ± 0.6 , 5.1 ± 1.0 and 4.6 ± 0.8 s (mean \pm SD), respectively. The peak time of LGN was significantly earlier than A17 ($p = 0.0047$, same or earlier in 8 out of 8 cats); the peak time between A17/A18 ($p = 0.28$) and A18/LGN ($p = 0.14$) were not significantly different. Generally, the BOLD response of LGN started 0.5 s earlier and peaked 0.8 s earlier than A17.

BOLD temporal frequency tuning curve and preference maps

To better visualize the difference in temporal frequency preference among A17, A18 and LGN of the isoflurane-anesthetized cats, normalized responses of four temporal frequencies and fitted

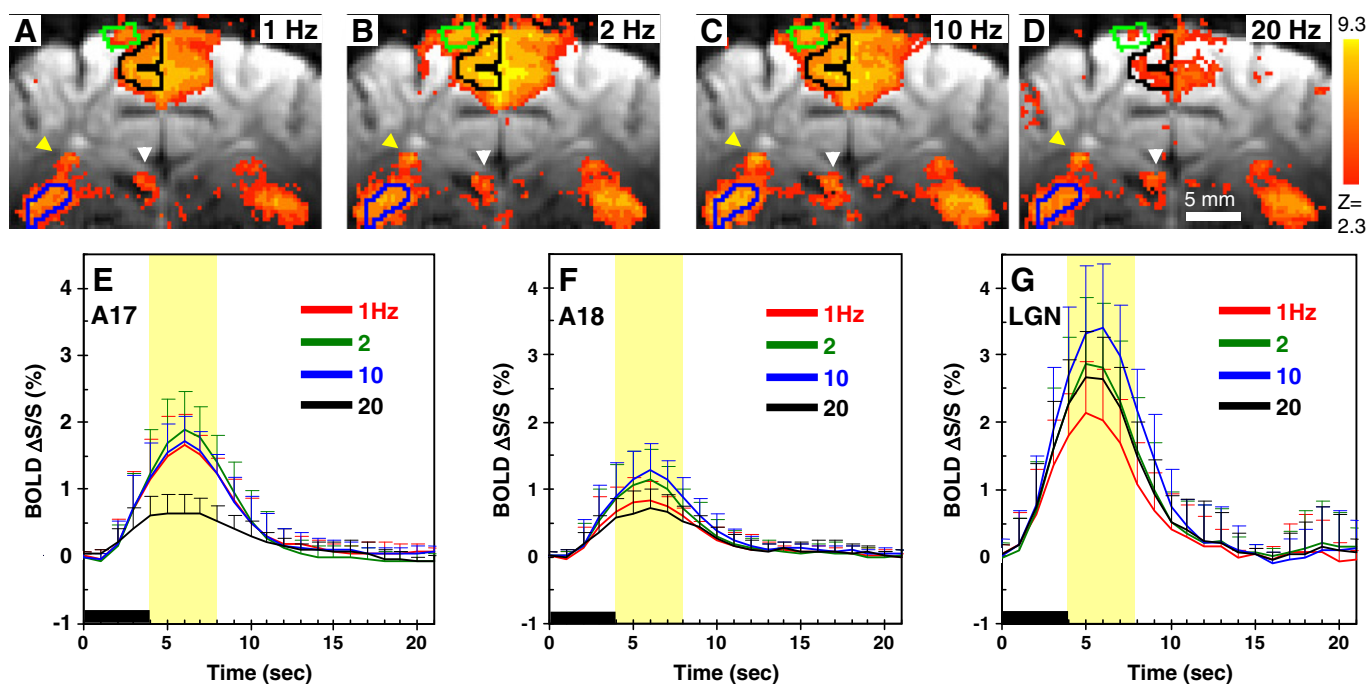


Fig. 2. Temporal frequency-dependent BOLD activation maps and time courses. (A–D) Spatial pattern of BOLD responses to 1 Hz (A), 2 Hz (B), 10 Hz (C) and 20 Hz (D) stimulation in one isoflurane-anesthetized cat. ROIs were shown in only one hemisphere for display. Blue contour: LGN; black contour: A17; green contour: A18. Medial white and lateral green arrowheads indicate superior colliculus and pulvinar, respectively. Color bar: Z-score value from 2.3 to 9.3 and higher. (E–G) Averaged BOLD time courses of A17 (E), A18 (F) and LGN (G) in all isoflurane-anesthetized animals responding to 1 Hz (red), 2 Hz (green), 10 Hz (blue) and 20 Hz (black) stimulation. The black bar spanning from 0 to 4 s indicates the stimulation period and the yellow-shaded area spanning from 5 to 8 s after stimulus onset is the period used for subsequent data analyses. Large error bars (standard deviations of 8 animals) are due to inter-animal variations.

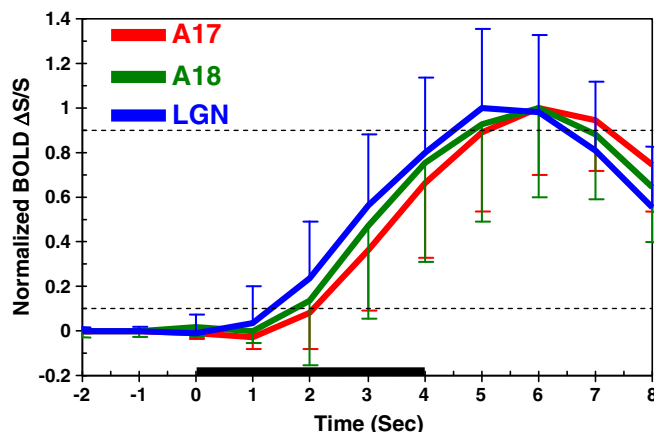


Fig. 3. Dynamic properties of BOLD responses in the early visual areas. Averaged, normalized BOLD time courses of A17 (red), A18 (green) and LGN (blue) in 8 isoflurane-anesthetized animals responding to 2 Hz stimulation were obtained. For clarity, only a 2-s pre-stimulus onset period and an initial 8-s post-stimulus onset period were plotted. The onset time was determined by the time to reach 10% of the peak amplitude (horizontal dashed line). Onset time of LGN response (1.8 ± 0.6 s) is significantly shorter than that of A17 (2.3 ± 0.4 s) and A18 (2.3 ± 0.7 s). The time to peak was determined by the time to reach 90% of the peak amplitude (horizontal dashed line). Peak time of LGN (4.6 ± 0.8 s) is significantly shorter than that of A17 (5.4 ± 0.6 s) and A18 (5.1 ± 1.0 s). Error bars = SD of 8 animals.

temporal frequency tuning curves (see Materials and methods) are shown in Fig. 4A. The Pearson's correlation coefficients (R) of the fitted Gaussian curves to the normalized BOLD responses for A17, A18 and LGN of eight cats were 0.86, 0.72 and 0.77, respectively. The preferred frequency of the tuning curve was 3.1 Hz for A17 (red), 4.5 Hz for A18 (green) and 6.0 Hz for LGN (blue). The bandwidth (full width at half maximum) of the tuning curve was 16 Hz for A17, 24 Hz for A18 and 52 Hz for LGN. Hence, A17 showed a lower preferred frequency and a narrower tuning bandwidth followed by A18 and LGN.

To determine the effect of anesthetics on the BOLD tuning curves and to compare the previously reported data obtained under sodium thiopental and fentanyl cocktail (Viswanathan and Freeman, 2007), we also determined and plotted average BOLD tuning curve of A17 in two animals under pentobarbital/fentanyl anesthesia (dashed line in Fig. 4B). Pentobarbital was used as an alternative to sodium thiopental, because sodium thiopental was discontinued by its manufacturer in the United States. Both thiopental and pentobarbital are short-acting barbiturate anesthetics that act on the GABA_A

receptor and pentobarbital is the main metabolite of sodium thiopental (Winters et al., 1955). Thus, the effect of pentobarbital on neural activity should be very similar to that of sodium thiopental. We observed that the BOLD preferred frequency (3.1 vs. 2.6 Hz) and tuning bandwidth (16 vs. 16 Hz) were similar between isoflurane and pentobarbital/fentanyl. The general trend of BOLD tuning curves was also similar ($R = 0.97$, p-value of two-tailed t-test = 0.03), regardless of anesthesia. Thus, we averaged all data including 8 isoflurane- and 2 pentobarbital/fentanyl-anesthetized studies for the comparison with previously reported neurophysiological data.

To examine the neural basis of fMRI, an A17 temporal frequency tuning curve of tissue pO₂, low frequency band of LFP (LFP_L: 0.7–12 Hz), gamma band of LFP (LFP_γ: 25–90 Hz) and spiking activity were adapted from data of Viswanathan and Freeman (2007) and plotted together with the BOLD tuning curve of A17 in Fig. 4C. Because the tuning curves of all low frequency bands of LFP, including LFP_δ(0.7–4 Hz), LFP_θ(4–8 Hz), and LFP_α(8–12 Hz), are almost indistinguishable, we considered all these low frequency components as one low frequency band and averaged them under the name LFP_L. The

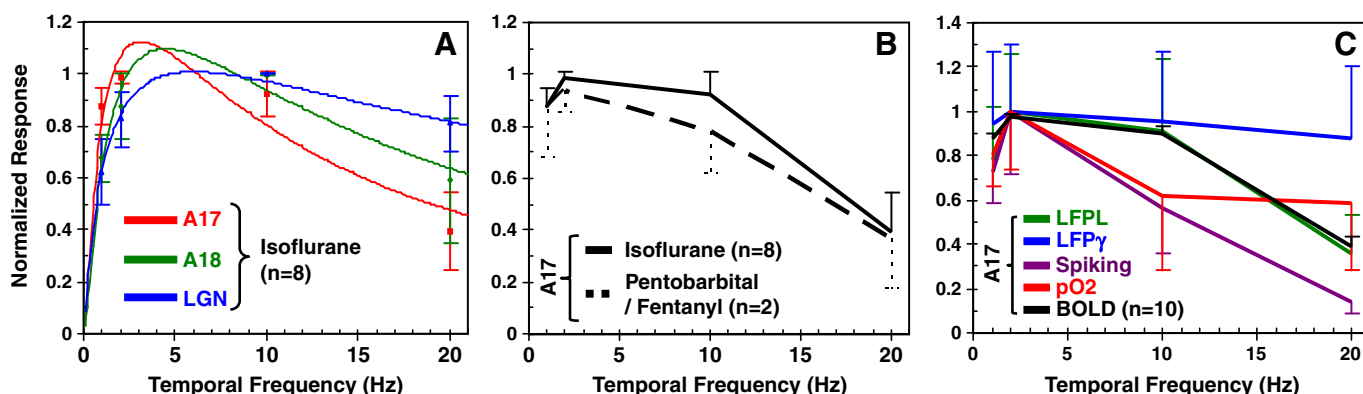


Fig. 4. Temporal frequency tuning curves of the early visual areas with BOLD fMRI, pO₂, LFP and spiking activity. (A) Normalized BOLD signals of A17 (red), A18 (green) and LGN (blue) in 8 isoflurane-anesthetized cats responding to four temporal frequencies were plotted as dots, in addition to the corresponding fitted tuning curve. The preference frequency determined from BOLD data agrees with one determined by electrophysiology (see texts) (Allison et al., 2001; Bisti et al., 1985; DeAngelis et al., 1993; Derrington and Fuchs, 1979). Error bars = SD of 8 animals. (B) Averaged frequency tuning curves of A17 in 8 isoflurane-anesthetized animals (solid lines) and 2 pentobarbital data (dashed line) were plotted for examining the effect of anesthesia. All data (n = 10) were averaged for comparison with neurophysiological data in (C). The tuning curve of the BOLD response of A17 (black) was plotted with that of tissue pO₂ (red), low frequency band (0.7–12 Hz) of LFP activity (LFP_L, green), middle-high frequency band (25–90 Hz) of LFP activity (LFP_γ, blue), and spiking activity (purple) adapted from Fig. 1 of Viswanathan and Freeman (2007). BOLD tuning curve more resembles LFP_L than LFP_γ, spiking activity and tissue pO₂ tuning curves. Error bars = SEM.

correlation coefficients and their corresponding p-value (two-tailed t-distribution) of BOLD tuning curve to LFP_L , LFP_γ , spiking activity and tissue pO_2 tuning curves were calculated: 0.98 ($p=0.017$), 0.95 ($p=0.050$), 0.92 ($p=0.078$) and 0.69 ($p=0.31$), respectively. Despite the small sampling size of 4, p-values give us a rough idea about the resemblance between these tuning curves. The BOLD tuning curve bears more resemblance to the LFP_L tuning curve compared to LFP_γ , spiking activity and tissue pO_2 tuning curves. The ratio between the response of 20 vs. 10 Hz stimuli for LFP_L , LFP_γ , spiking activity and tissue pO_2 were 0.49, 0.92, 0.25 and 0.94, respectively, while that of BOLD fMRI response was 0.44. This ratio again indicates that BOLD fMRI relates closer to LFP_L than LFP_γ , spiking activity and tissue pO_2 .

The preferred frequency can be used for differentiating A17 and A18. Fig. 5 shows preferred frequency maps of two representative cats where Figs. 5B and C are from the same cat in two different sessions. The similarity between Figs. 5B and C indicates that the temporal frequency preference map is reproducible across sessions. In A17 and A18 of both cats, the preferred frequency was around 3–4 Hz and 4–5 Hz, respectively. Within each cortical area, the distribution of the preferred frequency appears to be homogeneous from the cortical surface to the white matter, especially in A17. Due to limited number of frequencies, a preferred frequency cannot be robustly detected when the bandwidth of the tuning curve is large like LGN. Thus, the preferred frequency map in LGN looks inhomogeneous and discrete due to the inaccuracy of fitted values, exclusion of unreliable fittings, and contamination of large veins and white matter. At the ventral area outside of the A17 ROI, which represents a peripheral visual field, the preferred frequency appeared to be slightly higher than the majority of A17. The shifting was less obvious for A18 and might not be detectable in the current experimental protocol.

Discussion

Preferred temporal frequency in early visual systems

Temporal frequency is a fundamental visual feature. Detecting the regional temporal frequency preference in the visual system is an important step toward understanding and modeling the processing of visual information in the brain (Issa et al., 2008; Mullen et al., 2010). Furthermore, an impairment of the motion perception reflected in abnormal temporal frequency tuning properties may potentially serve for early detection of Alzheimer's disease or glaucoma (Nordmann et al., 1994). To distinguish fine changes in temporal frequency preferences, many temporal frequencies with a wide range should be used. However, only four temporal frequencies within 1–20 Hz range were used to obtain sufficient temporal SNR in our fMRI studies. In addition, we used a 2-mm slice thickness to obtain sufficient SNR resulting in partial

volume effects that might influence the magnitude of the BOLD response. In cortical area, the boundaries of gray matter, white matter and CSF are consistent over 2 mm, i.e. voxels containing non-gray matter are minimal within A17 and A18 ROIs as examined with 3-D venogram (slice thickness = 117 μ m, data not shown). On the other hand, we are aware that the LGN ROI may have a significant number of voxels containing white matter or vessels (Yen et al., 2010), because feline LGN is irregular in the caudal to rostral direction. However, the preferred frequency obtained from the BOLD response is still valid because the partial volume effect will change the BOLD magnitude similarly for all temporal frequency stimuli.

The cat primary visual cortex consists of cytoarchitectural subdivisions: A17 and A18. Although feline A17 and A18 conventionally relate to the primate V1 and V2, hierarchical processing in A17 and A18 is ambiguous in the cat and many other phylogenetically lower mammals compared to primate. For example, electrophysiological studies suggest that A17 and A18 contribute in complementary ways to visual processing of motion signals, such that A17 and A18 are responsible for encoding low and high temporal frequencies, respectively (Payne and Peters, 2002). Our temporal frequency tuning properties of BOLD responses in A17 and A18 may as well satisfy this notion. The preferred temporal frequency of A17 measured by BOLD fMRI (3.1 Hz) is comparable to that determined by electrophysiology (~3.8 Hz (Allison et al., 2001) and ~2.6 Hz (DeAngelis et al., 1993)), despite of the BOLD tuning curve of A17 having a wider bandwidth (16 Hz) than that of spiking activity (2.73 Hz) (Baker and Issa, 2005). Similarly, the preferred temporal frequency of A18 with BOLD fMRI (4.5 Hz) is consistent with electrophysiological findings (3–10 Hz) (Bisti et al., 1985). Despite the clear difference between A17 and A18 optimal temporal frequency, their tuning curves are largely overlapped.

LGN is a thalamic relay nucleus located between the retina and the primary visual cortex. LGN not only conveys retinal information to the cortex, but also receives feedback information from the cortex and other subcortical areas such as the superior colliculus. This is important for visual perception because LGN can influence the amount and nature of information relayed to the cortex (Chalupa et al., 2004). This dynamic control mechanism of LGN, if not suppressed by anesthesia, is one of the neural substrates of the visual attention (Chalupa et al., 2004). The preferred frequency of LGN measured by BOLD fMRI (6.0 Hz) falls within the range determined by electrophysiology (4 Hz–11 Hz) (Derrington and Fuchs, 1979). As seen in neural and BOLD responses, LGN is less selective to temporal frequencies of stimuli and can process relatively faster movements because of its higher tuning preference and broader tuning bandwidth. While cortical neurons fail to respond to high temporal frequency stimuli, LGN neurons respond well to such stimuli. The

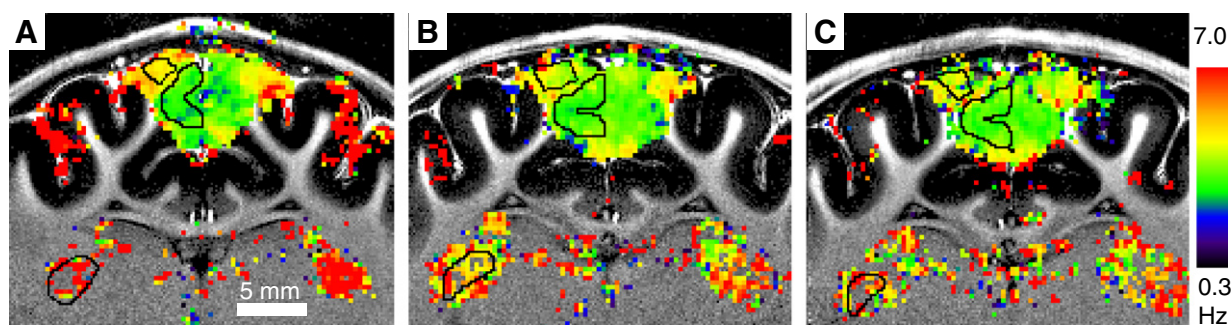


Fig. 5. Temporal frequency preference maps with BOLD fMRI. (A) and (B, C) are maps from two different animals whereas (B) and (C) are from the same animal in two different sessions. Color bar: preferred temporal frequency from 0.3 Hz (black) to 7 Hz and above (red). Black contours: A17, A18 and LGN. The preference maps of both animals show similar distribution of the preferred temporal frequency. The temporal frequency preference within our cortical ROIs (A17 and A18) is homogeneous indicating minimal sampling bias. Note that the peripheral visual field (lower edge of A17) shows higher temporal frequency preference.

reason for this behavior still remains unknown (Krukowski and Miller, 2001).

There are a few temporal frequency-dependent BOLD fMRI studies in animal visual cortex with diffuse flashing light instead of moving gratings (Pawela et al., 2008; Van Camp et al., 2006; Zhang et al., 2008). Note that the diffuse light source has no spatial pattern (spatial frequency = 0 cycle/degree), which evokes less cortical neural activity compared to moving grating stimulus (Rooney and Cooper, 1988). Zhang et al. (2008) varied the inter-stimulus interval (ISI) of flashing light-emitting diodes for their fMRI studies in cats, which could be considered as changing temporal frequency without the directional information. However, the stimulus duration was not fixed while varying the ISI in their cat studies; thus, it is difficult to compare their results to our findings. Van Camp et al. (2006) and Pawela et al. (2008) varied the flickering frequency of their diffuse light source with fixed stimulus duration in rats, but did not report frequency tuning properties. It would be interesting, if this information was available, to investigate the difference of tuning properties between cats and rats.

To examine the spatial distribution of the preferred frequency in the early visual system, the preferred frequency was determined on a voxel-by-voxel basis (Figs. 5A–C). In cortical areas, the preferred frequency is homogeneous within the ROI suggesting that our ROI-based analysis is not prone to sampling bias seen in most of the point-by-point electrophysiological recording techniques. At peripheral visual fields, there is an increment of temporal frequency preference that is not startling since the preferred temporal frequency increases abruptly at the peripheral visual field according to electrophysiological measurements (Orban et al., 1981). Note that the A17 ROI excluded these areas responsible for the peripheral vision. The shift of temporal frequency preference with retinal eccentricity may be better determined if a middle sagittal plane is used. In A18, the shift of temporal frequency preference between central and peripheral visual fields was not detectable in our BOLD fMRI studies, because this frequency shift was too small, as reported by electrophysiological recordings (Orban et al., 1981), to be detected by our stimulus paradigm.

Previously, several attempts have been made to map the temporal frequency preference in the visual cortex. Optical intrinsic signal (OIS) has been used to map the temporal frequency preference in monkeys (Khaytin et al., 2008) and cats (Ribot et al., 2008). Our result agrees with their findings that no significant difference in temporal frequency was observed across A17 except in the peripheral visual field. However, Sun et al. (2007) reported using fMRI that low and high temporal frequency domains were clustered separately in human visual cortex, which is inconsistent with our fMRI and OIS measurements (Khaytin et al., 2008; Ribot et al., 2008). The discrepancy may arise from the use of anesthesia in animal models or difference in species.

Dynamic property of visual evoked response in early visual system

We observed a faster onset of LGN BOLD response compared to the cortical response. Does this BOLD onset difference reflect the sequence of neural events? Electrophysiological measurements from the literature showed that the mean neural latency (95% confidence intervals in parenthesis) to LGN and A17 are 76 (70.2–82.2) and 104 (98.7–109.6) ms (Saul and Feidler, 2002). Since A17 are innervated by LGN directly, the neural onset time difference between LGN and A17 can be estimated by subtracting the latency of LGN from that of A17, which is about 28 ms. This timing difference is 18 times smaller than the onset time difference (500 ms) measured by BOLD fMRI. Hence, the difference of BOLD onset time between A17 and LGN cannot be interpreted simply as difference of neural activity onset time between these two areas. The sluggish BOLD response in A17 may attribute to different vascular reactivity (Wibral et al., 2007) and/or neurovascular coupling (Li and Freeman, 2007) in these two areas.

Relationships between BOLD and tissue pO_2

We have observed unexpected dissimilarity between our BOLD tuning and tissue pO_2 tuning curve measured by Viswanathan and Freeman (2007) especially at higher temporal frequency. The normalized BOLD response is 69% of the tissue pO_2 change at 20 Hz stimulation (Fig. 4C) and is even smaller at 30 Hz when linearly extrapolate both tuning curves. This discrepancy may be explained by a few possibilities as described below.

Firstly, the discrepancy may stem from difference between pO_2 and oxygen saturation level. It is often assumed that the change in tissue pO_2 is analogous to the BOLD response (Viswanathan and Freeman, 2007). Tissue pO_2 is determined by the oxygen diffusion gradient to the blood pO_2 , while the venous oxygen saturation level (S_vO_2) is related to the BOLD signal (Ogawa et al., 1998). Thus, the crucial link is whether blood pO_2 is linearly correlated with S_vO_2 . This relationship is described by the Hill equation of the oxygen dissociation curve with $P_{50} = 36.8$ mm Hg and $n = 3.207$ in cats (Herbert and Mitchell, 1971), with $S_vO_2 / (1 - S_vO_2) = (pO_2 / P_{50})^n$. To investigate the relationship between blood pO_2 and S_vO_2 , we assume tissue pO_2 is similar to blood pO_2 in microvessels. Since Viswanathan and Freeman (2007) only provided a relative pO_2 change of ~10% for a 2 Hz stimulus and ~6% for a 30 Hz stimulus, baseline tissue pO_2 in cats has to be taken from the literature. If the baseline tissue pO_2 is about 38.1 mm Hg (Nair et al., 1975), then the tissue pO_2 change of 10% and 6% corresponds to 3.8 mm Hg and 2.3 mm Hg, respectively. At this condition, the S_vO_2 change is approximately linear to tissue pO_2 . This corroborates with the argument that tissue pO_2 change is linearly correlated with the BOLD response. However, if the baseline tissue pO_2 is 12.8 mm Hg (Padnick et al., 1999), a change in pO_2 will be amplified more than the linear change in S_vO_2 in the supra-linear regime of the oxygen dissociation curve. When the S_vO_2 change is determined from 1.3 mm Hg (10% of baseline pO_2) and 0.77 mm Hg (6% of baseline tissue pO_2), for 2 and 30 Hz stimulations, then the relative change in S_vO_2 between the low frequency and high frequency responses is about 96% of the relative tissue pO_2 change. Thus, tissue pO_2 may no longer correlate linearly with the BOLD response. However, this non-linearity alone cannot explain the large difference (~69%) between the BOLD response and the tissue pO_2 change.

Secondly, the discrepancy may arise from CBV contribution to the BOLD signal. CBV is known to play an important role in the BOLD signal (Ogawa et al., 1998). If the CBV tuning curve is dramatically different from the tissue pO_2 tuning curve, then the BOLD tuning curve may diverge from the corresponding tissue pO_2 and CBV responses. However, this is unlikely to be the case, because our preliminary data indicates that the BOLD and CBV temporal frequency tuning curves are almost identical.

Thirdly, the discrepancy may be derived from the difference of anesthetics used. Both isoflurane (Masamoto et al., 2007) and barbiturate (Sanchez-Ferrer et al., 1985) dilate cerebral vessels and increase baseline cerebral blood flow. Cerebral blood flow, cerebral metabolic rate oxygen, mean arterial pressure and oxygen delivery are similar between these two anesthetics except that the cerebral vascular resistance is lower under isoflurane in human subjects (Newman et al., 1998). Most importantly, our preliminary results (Fig. 4B) showed that the BOLD tuning curves under pentobarbital/fentanyl and isoflurane were similar. Therefore, we do not think different anesthetics are the primary cause of the observed discrepancy between pO_2 and BOLD tuning curves.

Finally, point-by-point measurements of the tissue pO_2 which is sampled by oxygen sensors with areal sensitivity of $200 \mu m^2$ (Viswanathan and Freeman, 2007) are prone to sampling bias if the number of sampling points are limited, since tissue pO_2 is heavily influenced by the surrounding vasculature and the distance to the vessels (Nair et al., 1975). Thus, pO_2 data obtained from a limited

number of single-point measurements may differ from large volume data of fMRI. In summary, the interpretation of pO_2 measurement should be cautious when it is used as a BOLD analog.

Relationships between BOLD and neural activity

To address the neural source of the BOLD signal, we compared the frequency tuning curve of BOLD signal with that of the known neural activity components (Fig. 4C). Based on the correlation coefficient between these tuning curves, the trend of the BOLD tuning curve exhibits better resemblance to the LFP_L tuning curve than LFP_γ and spiking activity. Our result agrees with the findings of Maier et al. (2008) that BOLD correlates better with low frequency band of LFP (5–30 Hz) than spiking activity in the monkey's primary visual cortex during perceptual tasks. Our data also agrees with studies in human visual cortex, which show that the BOLD signal is better correlated with the low frequency band (below 40 Hz) of LFP using electroencephalography (Singh et al., 2003). Furthermore, Martuzzi et al. (2009) reported significant resemblance between the BOLD response and the low frequency band (<14 Hz) of LFP in human visual cortex using electroencephalography. However, they also reported the similarity between BOLD and gamma band (44–78 Hz) of LFP which corroborates with the finding in monkey visual cortex from Logothetis et al. (2001), but it disagrees with the result from Muthukumaraswamy and Singh (2008) that BOLD signal does not closely correlate with gamma band of LFP (40–60 Hz) using magnetoencephalography. Although our result shows more resemblance of the BOLD tuning curve to LFP_L tuning curve, it does not rule out the potential roles of LFP_γ and spiking activity in the basis of the BOLD fMRI. Our results shed insight into the complicated neural basis of the BOLD fMRI by providing evidences about closer relationship between BOLD response and LFP_L rather than LFP_γ or spiking activity.

Conclusions

We have successfully obtained the temporal frequency tuning curves of the early visual system in anesthetized cats using fMRI. In agreement with previous electrophysiological findings, BOLD fMRI was able to detect the subtle differences in the preferred temporal frequencies in A17, A18 and LGN. This implies that BOLD fMRI can show not only the location of the activation, but also the tuning property of the underlying neurons. We have also demonstrated that the BOLD signal of LGN increased earlier than that of A17 and A18 as known in the sequence of neural events. This hemodynamic onset time difference, however, is far larger than the neural onset time difference between LGN and A17/A18. Finally, we have demonstrated an apparent discrepancy between tuning curves of BOLD and tissue pO_2 responses, suggesting that tissue pO_2 measured point-by-point cannot simply represent the BOLD signal. Furthermore, the BOLD tuning curve was more similar to the low frequency band (<12 Hz) of LFP than the gamma band of LFP and spiking activity, indicating that cautious should be taken when interpret BOLD response as sole indicator of different aspect of the neural activity.

Acknowledgments

This work was supported by NIH grants EB003324, EB003375, and NS44589. We thank Ping Wang and Michelle Tasker for animal preparation, Kristy Hendrich for 9.4 T supports, Alberto Vazquez for calibrating high temporal frequency stimulation, and Alexander Poplawsky for editorial assistance. We are also grateful to Tao Jin, Alberto Vazquez, Kristy Hendrich and Alexander Poplawsky for helpful discussions.

References

- Abràmoff, M.D., Magalhaes, P., Ram, S., 2004. Image processing with ImageJ. *Biophotonics Int.* 11, 36–43.
- Allison, J.D., Smith, K.R., Bonds, A.B., 2001. Temporal-frequency tuning of cross-orientation suppression in the cat striate cortex. *Vis. Neurosci.* 18, 941–948.
- Baker, T.I., Issa, N.P., 2005. Cortical maps of separable tuning properties predict population responses to complex visual stimuli. *J. Neurophysiol.* 94, 775–787.
- Bandettini, P.A., Wong, E.C., Hinks, R.S., Tikofofsky, R.S., Hyde, J.S., 1992. Time course EPI of human brain-function during task activation. *Magn. Reson. Med.* 25, 390–397.
- Beckmann, C.F., Smith, S.M., 2004. Probabilistic independent component analysis for functional magnetic resonance imaging. *IEEE Trans. Med. Imaging* 23, 137–152.
- Bisti, S., Carmignoto, G., Galli, L., Maffei, L., 1985. Spatial-frequency characteristics of neurones of area 18 in the cat: dependence on the velocity of the visual stimulus. *J. Physiol.* 359, 259–268.
- Brainard, D.H., 1997. The psychophysics toolbox. *Spat. Vis.* 10, 433–436.
- Chalupa, L.M., Werner, J.S., Barnstable, C.J., 2004. *The Visual Neurosciences*. MIT press.
- DeAngelis, G.C., Ohzawa, I., Freeman, R.D., 1993. Spatiotemporal organization of simple-cell receptive fields in the cat's striate cortex. I. General characteristics and postnatal development. *J. Neurophysiol.* 69, 1091–1117.
- Derrington, A.M., Fuchs, A.F., 1979. Spatial and temporal properties of X and Y cells in the cat lateral geniculate nucleus. *J. Physiol.* 293, 347–364.
- Ekstrom, A., 2010. How and when the fMRI BOLD signal relates to underlying neural activity: the danger in dissociation. *Brain Res. Rev.* 62, 233–244.
- Haacke, E.M., Lindsokog, E.D., Lin, W., 1991. A fast, iterative, partial-fourier technique capable of local phase recovery. *J. Magn. Reson.* 92, 126–145.
- Heeger, D.J., Ress, D., 2002. What does fMRI tell us about neuronal activity? *Nat. Rev. Neurosci.* 3, 142–151.
- Herbert, D.A., Mitchell, R.A., 1971. Blood gas tensions and acid-base balance in awake cats. *J. Appl. Physiol.* 30, 434–436.
- Issa, N.P., Rosenberger, A., Husson, T.R., 2008. Models and measurements of functional maps in V1. *J. Neurophysiol.* 99, 2745–2754.
- Jesmanowicz, A., Bandettini, P.A., Hyde, J.S., 1998. Single-shot half k-space high-resolution gradient-recalled EPI for fMRI at 3 tesla. *Magn. Reson. Med.* 40, 754–762.
- Jin, T., Kim, S.G., 2008. Cortical layer-dependent dynamic blood oxygenation, cerebral blood flow and cerebral blood volume responses during visual stimulation. *Neuroimage* 43, 1–9.
- Khawaja, F.A., Tsui, J.M.G., Pack, C.C., 2009. Pattern motion selectivity of spiking outputs and local field potentials in macaque visual cortex. *J. Neurosci.* 29, 13702.
- Khaytin, I., Chen, X., Royal, D.W., Ruiz, O., Jermakowicz, W.J., Siegel, R.M., Casagrande, V. A., 2008. Functional organization of temporal frequency selectivity in primate visual cortex. *Cereb. Cortex* 18, 1828–1842.
- Kim, T., Kim, S.-G., 2011. Temporal dynamics and spatial specificity of arterial and venous blood volume changes during visual stimulation: implication for BOLD quantification. *J. Cereb. Blood Flow Metab.* 31, 1211–1222.
- Krukowski, A.E., Miller, K.D., 2001. Thalamocortical NMDA conductances and intracortical inhibition can explain cortical temporal tuning. *Nat. Neurosci.* 4, 424–430.
- Kwong, K.K., Belliveau, J.W., Chesler, D.A., Goldberg, I.E., Weisskoff, R.M., Poncelet, B.P., Kennedy, D.N., Hoppel, B.E., Cohen, M.S., Turner, R., Cheng, H.M., Brady, T.J., Rosen, B.R., 1992. Dynamic magnetic-resonance-imaging of human brain activity during primary sensory stimulation. *Proc. Natl. Acad. Sci. U. S. A.* 89, 5675–5679.
- Li, B., Freeman, R.D., 2007. High-resolution neurometabolic coupling in the lateral geniculate nucleus. *J. Neurosci.* 27, 10223–10229.
- Logothetis, N.K., Pauls, J., Augath, M., Trinath, T., Oeltermann, A., 2001. Neurophysiological investigation of the basis of the fMRI signal. *Nature* 412, 150–157.
- Maier, A., Wilke, M., Aura, C., Zhu, C., Ye, F.Q., Leopold, D.A., 2008. Divergence of fMRI and neural signals in V1 during perceptual suppression in the awake monkey. *Nat. Neurosci.* 11, 1193–1200.
- Martuzzi, R., Murray, M.M., Meuli, R.A., Thiran, J.P., Maeder, P.P., Michel, C.M., de Peralta, Grave, Menendez, R., Gonzalez Andino, S.L., 2009. Methods for determining frequency- and region-dependent relationships between estimated LFPs and BOLD responses in humans. *J. Neurophysiol.* 101, 491–502.
- Masamoto, K., Kim, T., Fukuda, M., Wang, P., Kim, S.-G., 2007. Relationship between neural, vascular, and bold signals in isoflurane-anesthetized rat somatosensory cortex. *Cereb. Cortex* 17, 942–950.
- Mitzdorf, U., 1985. Current source-density method and application in cat cerebral cortex: investigation of evoked potentials and EEG phenomena. *Physiol. Rev.* 65, 37.
- Moelker, A., Pattynama, P.M., 2003. Acoustic noise concerns in functional magnetic resonance imaging. *Hum. Brain Mapp.* 20, 123–141.
- Moisy, F., 2011. EzyFit — A Free Curve Fitting Toolbox for Matlab. <http://www.fast-upsud.fr/ezyfit/2011>.
- Mukamel, R., Gelbard, H., Arieli, A., Hasson, U., Fried, I., Malach, R., 2005. Coupling between neuronal firing, field potentials, and fMRI in human auditory cortex. *Science* 309, 951–954.
- Mullen, K.T., Thompson, B., Hess, R.F., 2010. Responses of the human visual cortex and LGN to achromatic and chromatic temporal modulations: an fMRI study. *J. Vis.* 10, 13.
- Muthukumaraswamy, S.D., Singh, K.D., 2008. Spatiotemporal frequency tuning of BOLD and gamma band MEG responses compared in primary visual cortex. *Neuroimage* 40, 1552–1560.
- Nair, P., Whalen, W.J., Buerk, D., 1975. PO_2 of cat cerebral cortex: response to breathing N_2 and 100 per cent O_2 . *Microvasc. Res.* 9, 158–165.
- Newman, M.F., Croughwell, N.D., White, W.D., Sanderson, I., Spillane, W., Reves, J.G., 1998. Pharmacologic electroencephalographic suppression during cardiopulmonary bypass: a comparison of thiopental and isoflurane. *Anesth. Analg.* 86, 246–251.

- Nordmann, J.P., Casanova, C., Denis, P., Savard, T., Saraux, H., 1994. Tuning properties of spatial and temporal channels of vision clinical consequences. *Neuroophthalmology* 14, 9–14.
- Ogawa, S., Tank, D.W., Menon, R., Ellermann, J.M., Kim, S.G., Merkle, H., Ugurbil, K., 1992. Intrinsic signal changes accompanying sensory stimulation – functional brain mapping with magnetic-resonance-imaging. *Proc. Natl. Acad. Sci. U. S. A.* 89, 5951–5955.
- Ogawa, S., Menon, R.S., Kim, S.G., Ugurbil, K., 1998. On the characteristics of functional magnetic resonance imaging of the brain. *Annu. Rev. Biophys. Biomol. Struct.* 27, 447–474.
- Orban, G.A., Kennedy, H., Maes, H., 1981. Response to movement of neurons in areas 17 and 18 of the cat: velocity sensitivity. *J. Neurophysiol.* 45, 1043–1058.
- Padnick, L.B., Linsenmeier, R.A., Goldstick, T.K., 1999. Oxygenation of the cat primary visual cortex. *J. Appl. Physiol.* 86, 1490–1496.
- Park, S.H., Masamoto, K., Hendrich, K., Kanno, I., Kim, S.G., 2008. Imaging brain vasculature with BOLD microscopy: MR detection limits determined by in vivo two-photon microscopy. *Magn. Reson. Med.* 59, 855–865.
- Pawela, C.P., Hudetz, A.G., Ward, B.D., Schulte, M.L., Li, R., Kao, D.S., Mauck, M.C., Cho, Y. R., Neitz, J., Hyde, J.S., 2008. Modeling of region-specific fMRI BOLD neurovascular response functions in rat brain reveals residual differences that correlate with the differences in regional evoked potentials. *Neuroimage* 41, 525–534.
- Payne, B.R., Peters, A., 2002. *The Cat Primary Visual Cortex*. Academic Press, San Diego.
- Rees, G., Friston, K., Koch, C., 2000. A direct quantitative relationship between the functional properties of human and macaque V5. *Nat. Neurosci.* 3, 716–723.
- Reinoso-Suárez, F., 1961. *Topographischer Hirnatlas der Katze für experimental-physiologische Untersuchungen*. E. Merck AG, Darmstadt.
- Ribot, J., Ozawa, K., Tani, T., Milleret, C., Tanaka, S., 2008. Program No. 366.1. Spatio-temporal frequency preference map in cat primary visual cortex. *Neuroscience Meeting Planner. Society for Neuroscience*, Washington, DC. Online.
- Rooney, B.J., Cooper, R.M., 1988. Effects of square-wave gratings and diffuse light on metabolic activity in the rat visual system. *Brain Res.* 439, 311–321.
- Rorden, C., Karnath, H.O., Bonilha, L., 2007. Improving lesion-symptom mapping. *J. Cogn. Neurosci.* 19, 1081–1088.
- Sanchez-Ferrer, C., Marin, J., Salaices, M., Rico, M., Munoz-Blanco, J., 1985. Interference of pentobarbital and thiopental with the vascular contraction and noradrenaline release in human cerebral arteries. *Gen. Pharmacol. Vasc. Syst.* 16, 469–473.
- Saul, A.B., Feidler, J.C., 2002. Development of response timing and direction selectivity in cat visual thalamus and cortex. *J. Neurosci.* 22, 2945–2955.
- Singh, M., Kim, S., Kim, T.S., 2003. Correlation between BOLD-fMRI and EEG signal changes in response to visual stimulus frequency in humans. *Magn. Reson. Med.* 49, 108–114.
- Smith, S.M., Jenkinson, M., Woolrich, M.W., Beckmann, C.F., Behrens, T.E.J., Johansen-Berg, H., Bannister, P.R., De Luca, M., Drobnjak, I., Flitney, D.E., Niazy, R.K., Saunders, J., Vickers, J., Zhang, Y.Y., De Stefano, N., Brady, J.M., Matthews, P.M., 2004. Advances in functional and structural MR image analysis and implementation as FSL. *Neuroimage* 23, S208–S219.
- Strupp, J., 1996. Stimulate: a GUI based fMRI analysis software package. *Neuroimage* 3 [S607-S607].
- Sun, P., Ueno, K., Waggoner, R.A., Gardner, J.L., Tanaka, K., Cheng, K., 2007. A temporal frequency-dependent functional architecture in human V1 revealed by high-resolution fMRI. *Nat. Neurosci.* 10, 1404–1406.
- Van Camp, N., Verhoye, M., De Zeeuw, C.I., Van der Linden, A., 2006. Light stimulus frequency dependence of activity in the rat visual system as studied with high-resolution BOLD fMRI. *J. Neurophysiol.* 95, 3164–3170.
- Vazquez, A.L., Fukuda, M., Tasker, M.L., Masamoto, K., Kim, S.G., 2010. Changes in cerebral arterial, tissue and venous oxygenation with evoked neural stimulation: implications for hemoglobin-based functional neuroimaging. *J. Cereb. Blood Flow Metab.* 30, 428–439.
- Viswanathan, A., Freeman, R.D., 2007. Neurometabolic coupling in cerebral cortex reflects synaptic more than spiking activity. *Nat. Neurosci.* 10, 1308–1312.
- Wibral, M., Muckli, L., Melnikovic, K., Scheller, B., Alink, A., Singer, W., Munk, M.H., 2007. Time-dependent effects of hyperoxia on the BOLD fMRI signal in primate visual cortex and LGN. *Neuroimage* 35, 1044–1063.
- Winters, W., Spector, E., Wallach, D., Shideman, F., 1955. Metabolism of thiopental-S35 and thiopental-2-C14 by a rat liver mince and identification of pentobarbital as a major metabolite. *J. Pharmacol. Exp. Ther.* 114, 343.
- Yen, C.C.-C., Fukuda, H., Kim, S.-G., 2009. Temporal Frequency- and Time-dependent BOLD and CBV fMRI Signals in Cat Visual Areas 17 and 18. *International Society for Magnetic Resonance in Medicine*, Honolulu.
- Yen, C.C.-C., Fukuda, H., Kim, S.-G., 2010. The Spatiotemporal Characteristics of Visual Stimulus-Induced BOLD Responses in Cat Visual Areas. *International Society for Magnetic Resonance in Medicine*, Stockholm, Sweden.
- Zhang, N., Zhu, X.H., Zhang, Y., Chen, W., 2008. An fMRI study of neural interaction in large-scale cortico-thalamic visual network. *Neuroimage* 42, 1110–1117.